Optical and Quantum Electronics (2019) 51:145
https://doi.org/10.1007/s11082-019-1868-y

Photoelectron holographic interferences from multiple returning in strong-field tunneling ionization

Yali Liu[1] · Jia Tan[1] · Mingrui He[1] · Hui Xie[1] · Yanan Qin[1] · Yong Zhao[1] · Min Li[1] · Yueming Zhou[1] · Peixiang Lu[1,2]

Received: 19 March 2019 / Accepted: 24 April 2019

Abstract
By numerically solving the time-dependent Schrödinger equation, we theoretically investigate the holographic structure of the multiple-returning rescattering recorded in the photoelectron momentum distribution. In the orthogonally polarized two-color fields, we show that the interference patterns periodically oscillate with the relative phase. Tracing the relative phase where the oscillation minimizes, we find that the dependences of the phase on the parallel momentum for the first-returning and the second-returning rescattering holographic interferences are different. With the quantum-orbit model, we demonstrated that the difference is related to the ionization and rescattering times of the electron. Moreover, we show that the influence of the Coulomb interaction on the oscillation of both the first-returning rescattering and the second-returning rescattering holographic interferences can be ignored. This suggests us that the temporal characteristics of the electron can be resolved by analyzing the relative phase's dependence of the multiple-returning holographic interference.

Keywords Above-threshold ionization · Strong laser field · Photoionization of atoms and ions

1 Introduction

The atoms or molecules exposed to a strong laser field can be tunneling ionized and produce an electron wave packet (EWP) (Becker et al. 2002; Corkum 1993; Krausz and Ivanov 2009; Liu et al. 2019; Qin et al. 2019; Wang et al. 2019). The released EWP is further accelerated by the oscillating electric field of laser pulse and may be driven back toward the core, giving rise to various nonlinear phenomena, such as above-threshold ionization (Kang et al. 2010; Paulus et al. 1994; Salières et al. 2001), high-order harmonic generation (Gaarde and Schafer 2002; He et al. 2018; He et al. 2019; Ferray et al. 1988; Krause et al. 1992; Li et al. 2019a, b; Li et al. 2018; Zhai et al. 2019; Zhang et al. 2019) and nonsequential double ionization (Ma et al. 2018, 2019; Tong et al. 2019; Walker et al. 1994;

✉ Yueming Zhou
zhouymhust@hust.edu.cn

Extended author information available on the last page of the article

Published online: 29 April 2019

Zhou et al. 2011a, b). Due to the coherent nature, the ionized EWP that undergoes different pathways achieving the same final momentum interferes with each other, inducing the rich interference patterns in the final photoelectron momentum distribution (PEMD). Generally, the interference patterns could be classified into two categories. The first category is the intercycle interference with the EWPs released at time intervals separated by the laser cycles, which leads to the above-threshold ionization (ATI) peaks. The second category is the intracycle interference arising from the EWPs launched within the adjacent half cycles (Arbó et al. 2006, 2014; Lindner et al. 2005; Xie et al. 2012). For this interference, the one EWP drifts to the detector directly without further interaction with the target ion (direct EWP), and for the other one, its direction is reversed in the laser field.

After tunneling ionization, the rescattering EWP with the same final momentum as the direct one results in another important interference, i.e, strong-field photoelectron holography (Bian et al. 2011; Du et al. 2016; Huismans et al. 2011, 2012). This structure is analogy to the optical holography (Gabor 1948) and it has been extensively studied for different targets in many experiments (Arbó et al. 2015; Hickstein et al. 2012; Huismans et al. 2012; Meckel et al. 2014); Li et al. accepted). In previous works, with this holographic interference we have extracted the phase of the scattering amplitude of the atoms (Zhou et al. 2016). Recently, from this interference we have measured the charge migration of molecules in real time and in situ with attosecond temporal resolution (He et al. 2018). Very recently, we have proposed that the time information for tunneling ionization can be resolved by analyzing this holographic interference (Tan et al. 2018a).

For the above holographic interference, the EWP is rescattered by the nucleus at its first returning. In fact, the rescattering can also occur at its second or third returnings (Faisal 2009; Liu and Hatsagortsyan 2010; Yan et al. 2010). For example, a low-energy structure which was regarded as the "ionization surprise" was found in the mid-infrared laser fields (Faisal 2009). This low-energy structure is theoretically considered to originate from the rescattering at the multiple returnings (Blaga et al. 2009; Quan et al. 2009). Recently, numerous studies have shown that the direct EWPs may interfere with these multiple-returning rescattering EWPs resulting in the multiple-returning holographic interference in the low-energy region of photoelectron momentum distribution (PEMD) (Liu and Hatsagortsyan 2010; Xie et al. 2016; Yan et al. 2010). Specially, it has been demonstrated that the distance between electrons and nucleus during tunneling can be obtained by analyzing the cut-off energy of this structure (Hickstein et al. 2012). Recently, it has been pointed out that this multiple-returning rescattering structure can act as a tool for studying the attosecond dynamics of atoms and molecules (Agueny and Hansen 2018). While for this structure, how to measure the temporal characteristics of the electron in tunneling ionization process has still not studied.

In this paper, we theoretically study the multiple-returning holographic interferences of the PEMD for the Xe atom in strong-field tunneling ionization. In the work, the atom is ionized by the orthogonally polarized two-color (OTC) fields consisting of a weak second harmonic and a strong fundamental field. Our result indicates that the holographic interference fringes oscillate with the relative phase of this two-color fields and this oscillation corresponds to the parallel momentum. Monitoring the position of the interference maximum and tracing the relative phase where the oscillation of the interference fringes minimize, we find that the dependence of the phase on parallel momentum for both the first-returning rescattering and the second-returning rescattering holographic interferences are different. With the quantum-orbit model, we demonstrated that this difference is related to the ionization and rescattering times of the electron. Additionally, the good agreement between the quantum-orbit model results and TDSE calculations confirms that the influence of Coulomb interaction on the oscillation of

both the first-returning and the second-returning holographic interferences can be neglected. This suggests that analyzing the dependence of the position of the multiple-returning rescattering holographic interference on the relative phase allows us to measure the temporal information of the electron in tunneling ionization.

2 Theoretical methods

2.1 Numerically solving the TDSE

A fully quantum method based on solving the two-dimensional TDSE is used to obtain the PEMD,

$$i\frac{\partial}{\partial t}\Psi(\mathbf{r},t) = H(\mathbf{r},t)\Psi(\mathbf{r},t). \tag{1}$$

Here, $\Psi(\mathbf{r},t)$ is the electron wave function. The Hamiltonian $H(\mathbf{r},t)$ is written as

$$H(\mathbf{r},t) = -\frac{1}{2}\bigtriangledown^2 + V(\mathbf{r}) + \mathbf{r}\cdot\mathbf{E}(t), \tag{2}$$

where $\mathbf{r}$ represents the position coordinate of electron and $V(\mathbf{r}) = -1/\sqrt{x^2+y^2+a}$ is the Coulomb potential. For Xe atom, the soft-core parameter is set as 0.92 to correctly reproduce the ground-state energy. The electric field is $\mathbf{E}(t) = f(t)[E_0\cos(\omega t)\hat{\mathbf{e}}_x + E_1\cos(2\omega t+\phi)\hat{\mathbf{e}}_y]$. E_0 represents the amplitude of 1300-nm field which polarizes along the x axis and E_1 denotes the amplitude of the 650-nm field which is polarized along the y axis. The intensities of the 1300-nm and 650-nm fields are 1.5×10^{14} W/cm^2 and 1.0×10^{12} W/cm^2, respectively. ϕ indicates the relative phase of this OTC fields. $f(t)$ denotes the trapezoidal pulse envelope, rising in the first cycle, remaining constant in the second to fourth cycle, and falling in the last cycle of the 1300-nm pulse. For this OTC fields, the TDSE is solved by the method of split-operator spectral on a Cartesian grid (Feit et al. 1982). The Cartesian grid ranges from −400 a.u. to 400 a.u. with the grid and the spatial discretization is $\Delta x = \Delta y = 0.2$ a.u. The time step $\Delta t = 0.045$ a.u.

2.2 Quantum-orbit model

With quantum-orbit model, we investigate the holographic interference pattern of the PEMDs. This holographic structure derives from the interference of the direct and the rescattering electrons and it can be expressed as $M^2 = (M_d + M_r)^2 = M_d^2 + M_r^2 + 2M_dM_rcos(\Delta\theta)$, where M_d is the amplitudes of the direct electrons, M_r is the amplitudes of the rescattering electrons and $\Delta\theta$ is the phase difference of these two types electrons. According to Tan et al. (2018a, b), $\Delta\theta$ for the OTC fields is written as

$$\Delta\theta(\phi) = \frac{1}{2}[p_\perp - k_\perp(\phi)]^2(t_r - t_i) + \alpha. \tag{3}$$

Here, $k_\perp(\phi) = -\int_{t_i}^{t_r} A_\perp(t;\phi)dt/(t_r - t_i)$ is the transverse component of the canonical momentum $\mathbf{k}$. $p_\perp$ represents the transverse component of the electron final momentum $\mathbf{p}$. α is the phase of the rescattering amplitude introduced in Zhou et al. (2016). t_r is the

rescattering time of the rescattering electron and t_i represents the ionization time of the direct electron.

In our study, the 650-nm field of the OTC fields is very weak relative to the 1300-nm field. Thus we can approximately obtain the ionization and rescattering times by solving the saddle-point equations in the 1300 nm field only. The saddle-point equations are written as Huismans et al. (2011), Salières et al. (2001), Tan et al. (2018b).

$$\frac{1}{2}[\mathbf{p} + A_x(t_i^d)]^2 + I_p = 0, \tag{4}$$

$$\frac{1}{2}[k_x + A_x(t_i^r)]^2 + I_p = 0, \tag{5}$$

$$\frac{1}{2}[k_x + A_x(t_r)]^2 = \frac{1}{2}[\mathbf{p} + A_x(t_r)]^2, \tag{6}$$

$$\int_{t_i^r}^{t_r} [\mathbf{k} + \mathbf{A}(t)]dt = 0, \tag{7}$$

It should be noted that in the following the superscript of t_i is omitted, since $t_i^r \doteq t_i^d$ for the near-forward rescattering (He et al. 2018).

3 Results and discussions

In Fig. 1, we present the PEMDs calculated by TDSE for Xe in the 1300-nm laser field and the OTC laser fields consisting of a strong 1300-nm laser field and a weak 650-nm laser field with relative phase $\phi = 0.5\pi$, respectively. The laser intensities of the 1300-nm field and the 650-nm field are 1.5×10^{14} W/cm^2 and 1.0×10^{12} W/cm^2. In Fig. 1a and b, one can see two types of spider-like patterns clearly. The one in the momentum region of $|p_x| \geqslant 0.6$ a.u. is the first-returning holographic pattern coming from the interference of the direct electrons and the electrons scattered by the nucleus at the first returning (Huismans et al.

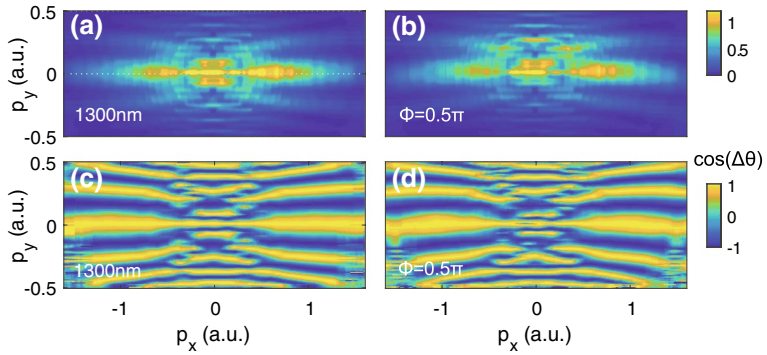

Fig. 1 **a** The PEMD for Xe atom calculated by TDSE in a 1300-nm single-color laser field. **b** The same as **a** but for the PEMD in the OTC fields consisting of a 1300-nm pulse and a 650-nm pulse with relative phases $\phi = 0.5\pi$. **c** and **d** The interference term $\cos(\Delta\theta)$ extracted from **a** and **b**, respectively. (Color figure online)

2011). The other one, in the momentum region of $|p_x| \leqslant 0.3$ a.u., is the second-returning holographic structure deriving from the direct electrons and the electrons rescattering at the second returning (Hickstein et al. 2012). For the 1300-nm field, these two types of holographic fringes are symmetric with respect to the p_x axis and the p_y axis. For the OTC laser fields, these interference fringes are also symmetric with respect to the p_y axis, while for the p_x axis the interference fringes are disturbed by the SH component of the OTC fields, resulting in the shift.

Using the procedure demonstrated in Zhou et al. (2016), we extract the interference term $\cos(\Delta\theta)$ of the holographic pattern from the PEMDs. Figure 1c and d present the obtained results for $p_x \in [-1.6, 1.6]$ a.u. In the OTC fields, the first-returning and the second-returning holographic fringes are shifted along p_y direction with respect to that of the 1300-nm field. This is more obvious in Fig. 2a and b where we present several cuts of $\cos(\Delta\theta)$ for the second-returning and the first-returning holographic fringes in the 1300-nm field and the OTC fields, respectively. For the cut of $p_x = -0.2$ a.u., corresponding to the second-returning rescattering holographic interference fringes, the interference maxima shift right at $\phi = 0$ and shift left at $\phi = \pi$ with respect to 1300-nm field. For the cut of $p_x = -1.2\pi$ which corresponds to the first-returning rescattering holographic interference, this shift is also related to the relative phase. In Tan et al. (2018b), the shift of the first-returning holographic fringes has been found and studied. In the following, we will reveal the originate of the second-returning holographic fringes.

To describe the shift Δp_y of the holographic interference fringes quantitatively, we monitored the position of the zeroth maximum of $\cos(\Delta\theta)$ in the OTC fields and extract its shift Δp_y relative to that of the 1300-nm field. Figure 2c presents the obtained Δp_y as a function of ϕ at $p_x = -0.1$ a.u. and $p_x = -0.25$ a.u., respectively. It is shown that depending on p_x, Δp_y periodically oscillates with ϕ. For example, for $p_x = -0.1$ a.u., Δp_y maximizes at $\phi = 2.2\pi$ and for $p_x = -0.25$ a.u., it maximizes at $\phi = 2\pi$. As a comparison, we also present Δp_y for the first-returning holographic fringes at $p_x = -0.8$ a.u. and $p_x = -1.5$ a.u.

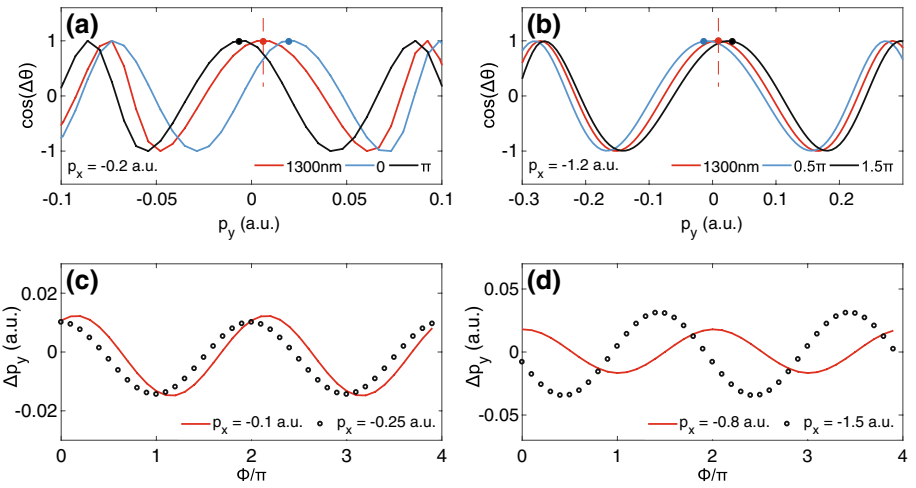

Fig. 2 **a** The $\cos(\Delta\theta)$ at $p_x = -0.2$ a.u. The red line indicates the result of the 1300-nm field. The blue and black lines indicate the data for the OTC fields with $\phi = 0$ and $\phi = \pi$, respectively. **b** The same as **a** but at $p_x = -1.2$ a.u. **c** The shift Δp_y of zeroth maximum of $\cos(\Delta\theta)$ as a function of ϕ at $p_x = -0.1$ a.u. (red solid curves) and $p_x = -0.25$ a.u. (black circles). **d** The same as **c** but at $p_x = -0.8$ a.u. (red solid curves) and $p_x = -1.5$ a.u. (black circles). (Color figure online)

as indicated in Fig. 2d. It is shown that Δp_y varies with ϕ and the phase ϕ where Δp_y minimizes changes with p_x. This is more clearly seen in Fig. 3a and b, in which we present Δp_y as a function of ϕ for $p_x \in [-1.6, -0.6]$ a.u. and $p_x \in [-0.3, -0.1]$ a.u. These two ranges correspond to the first-returning and the second-returning rescattering holographic interference, respectively. It is displayed that the relative phase where Δp_y minimizes is sensitive to the parallel momentum.

We calculate Δp_y of the position of the zeroth maxima for the first-returning and the second-returning holographic fringes with Eq. (3). Equation (3) has been pointed out in Tan et al. (2019). According to this equation, the position of the maximum of the holographic pattern in the OTC fields is obtained by

$$p_\perp^{OTC} = \sqrt{2[\Delta\theta(\phi) + \alpha]/(t_r - t_i)} + k_\perp(\phi), \tag{8}$$

where $k_\perp(\phi) = -\int_{t_i}^{t_r} A_\perp(t;\phi)dt/(t_r - t_i)$. For the 1300-nm field, the position of the maximum locates at

$$p_\perp^{SC} = \sqrt{2[\Delta\theta(\phi) + \alpha]/(t_r - t_i)}, \tag{9}$$

where $\Delta\theta(\phi) = 0, 2\pi, 4\pi...$ for the zeroth maximum, the first maximum, the second maximum and the later maxima of the interference fringes, respectively. It should be mentioned that the scattering amplitude phase α in the OTC fields is the same as that in the 1300-nm field since the additional second harmonic is a weak perturbation. Therefore, the shift Δp_y is obtained by

$$\Delta p_y = p_\perp^{OTC} - p_\perp^{SC} = k_\perp(\phi). \tag{10}$$

Equation (10) indicates that the shift of the zeroth maximum of the holographic fringes induced by the OTC fields equals to $k_\perp$, and it is related to ϕ of this OTC fields and also to p_x through t_i and t_r. For the first-returning holographic interference fringes, the prediction of Eq. (10) is shown in Fig. 3c, and for the second-returning holographic interference fringes, the prediction obtained from Eq. (10) is indicated in Fig. 3d. It is observed that the

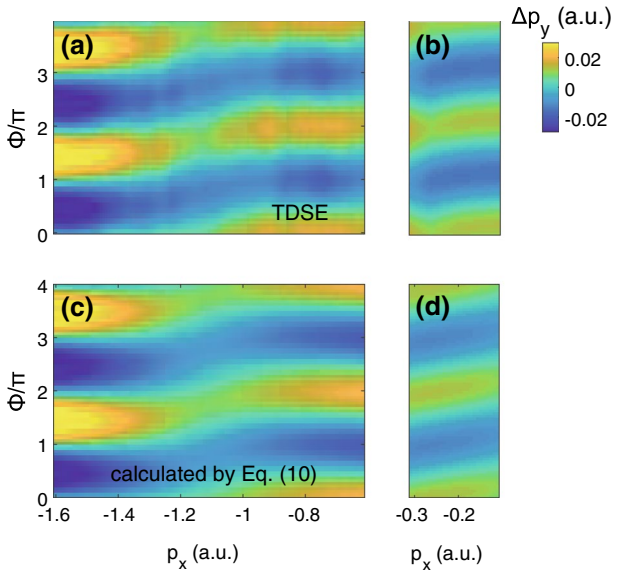

Fig. 3 **a** and **b** The shift Δp_y of the holographic interference fringe extracted from the TDSE results as a function of relative phase ϕ for $p_x \in [-1.6, -0.6]$ a.u. and $p_x \in [-0.3, -0.1]$ a.u., respectively. **c** and **d** The same as **a** and **b** but calculated by Eq. (10)

result of Fig. 3c agrees well with the TDSE calculation in Fig. 3a, and the data of Fig. 3d shows a good agreement with the TDSE calculation in Fig. 3b.

The periodic oscillation of Δp_y of the holographic fringes in Fig. 3 suggests to us fo fit Δp_y with

$$\Delta p_y = P_m \cos(\phi + \Phi_m), \tag{11}$$

where P_m indicates the amplitude of the oscillation and Φ_m represents the phase where the shift Δp_y minimizes. In our previous papers, we have shown that the quantities P_m and Φ_m could be used to retrieve the temporal characteristics of the electron and to determine the intensity of the laser field (Tan et al. 2018a, b). Here, we focus on the quantity Φ_m. The obtained results are displayed in Fig. 4a. It is shown that Φ_m of the TDSE calculation extracted from Fig. 3a and b changes from 2.4π to 3π when $p_x \in [-1.6, -0.6]$ a.u., and it changes from 2.95π to 3.15π when $p_x \in [-0.3, -0.1]$ a.u. As a comparison, we also present the phase Φ_m calculated by Eq. (10) for the first-returning holographic pattern and the second-returning holographic pattern in the momentum region $p_x \in [-1.6, -0.6]$ a.u. and $p_x \in [-0.3, -0.1]$ a.u. as shown in Fig. 4a, respectively. Clearly, in the momentum region $p_x \in [-1.6, -0.6]$ a.u., the predicted result by Eq. (10) for the first-returning holographic interference agrees well with the TDSE calculation. In the momentum region $p_x \in [-0.3, -0.1]$ a.u., the prediction for the first-returning holographic interference deviates from the TDSE calculation seriously, while the result for the second-returning holographic interference is in good agreement with the TDSE calculation. This indicates that the shift of the interference in the momentum region $p_x \in [-1.6, -0.6]$ comes from the first-returning holographic pattern and the shift in the region $p_x \in [-0.3, -0.1]$ originates from the second-returning holographic pattern. We should mention that for Eq. (10), the Coulomb interaction is not included. Therefore, the agreement between the TDSE calculation and the result of Eq. (10) confirms that the Coulomb interaction is negligible for the shift of the holographic interference.

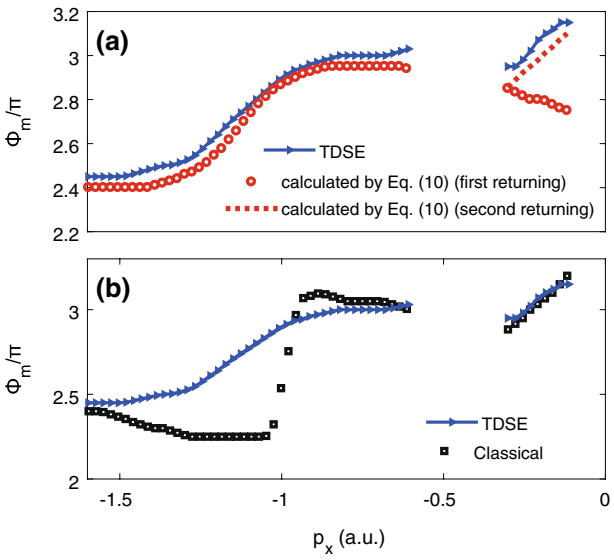

Fig. 4 The phase Φ_m as a function of p_x.The blue triangles represent the data extracted from the TDSE result. The red circles and red dots denote the data calculated by Eq. (10) for the first-returning and second-returning holographic interference fringes, respectively. The black squares represent the result of the classical model. (Color figure online)

In the momentum region $p_x \in [-0.3, -0.1]$ a.u., the prediction for the first-returning holographic interference fringes decreases with the parallel momentum p_x increases, while for the second-returning holographic interference fringes, it increases with p_x increases. The difference is due to the ionization and rescattering times obtained by the saddle-point equations for the first-returning and the second-returning holographic fringes are different (Xie et al. 2016). This indicates that one is able to resolve the time information of the electron in tunneling ionization by analyzing the response of the first-returning and the second-returning holographic interference to the SH component of the OTC fields (Agueny and Hansen 2018; Tan et al. 2019).

We further compare $\boldsymbol{\Phi}_m$ of the TDSE results with that predicted by the classical models [with setting the ionization potential $I_p = 0$ in Eqs. (4) and (5)] as shown in Fig. 4b. It is clearly shown that for the first-returning holographic pattern in the momentum region $p_x \in [-1.6, -0.6]$ a.u., the result of the classical model deviates obviously from the TDSE result. While for the second-returning holographic pattern, in the momentum region $p_x \in [-0.3, -0.1]$ a.u., it agrees well with the TDSE result. This is because that the ionization for the second-returning holographic interference is near the maximum of the electric crest and thus the calculated ionization time by the classical model is very close to the result of the quantum-orbit model (Lein 2012; Shar et al. 2012; Smirnova et al. 2009; Tan et al. 2018a). While for the first-returning ones, the ionization time from the classical model deviate seriously from those of the quantum-orbit model and thus the calculated quantity $\boldsymbol{\Phi}_m$ is very different from that of the quantum-orbit model and the TDSE. These results indicate the quantity $\boldsymbol{\Phi}_m$ is very sensitive to the ionization time. Thus, the ionization time could be accurately extracted with our scheme.

In Fig. 5a, we present the PEMD for Xe atom in a 2000-nm laser field. It has been demonstrated that the multiple-returning holographic structure is favorably observed at the mid-infrared laser pulses (Marchenko et al. 2011). Here, to show this, we display the enlarged view of the momentum region in the momentum region $p_x \in [-1.2, 0]$ a.u. marked by the white box of Fig. 5a in b. It is indicated that the multiple-returning holographic structure is abundant and obviously visible in region II. This demonstrates that for a longer laser pulse, the second-returning or the multiple-returning holographic interference could be accurately extracted from the PEMD, and thus by studying the shift of multiple-returning interference fringes when a weak SH field is added, the temporal characteristics of electron in tunneling ionization can be resolved.

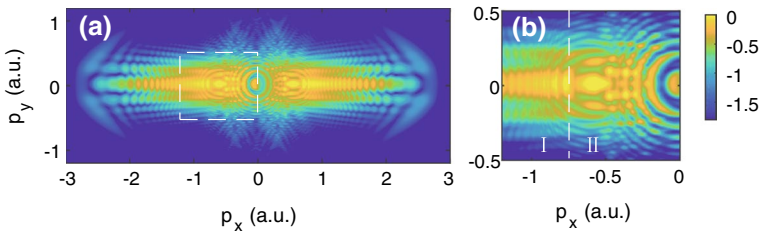

Fig. 5 **a** The PEMD for Xe in a 2000-nm laser field with the laser intensity 1.2×10^{14} W/cm^2. **b** The enlarged view of the momentum region marked by the white box in **a**. The dotted line divides the momentum region of **b** into two parts: I and II

4 Conclusion

We have studied the multiple-returning holographic interference of the PEMDs of Xe atom in the OTC fields. Our results showed that the first-returning and the second-returning holographic interference fringes oscillate with the changing of the relative phase of the OTC fields and this oscillation is sensitive to the parallel momentum. Tracing the relative phase where the oscillation of the interference fringes minimize, we find that the parallel momentum dependences of this phase are different for the first-returning and the second-returning rescattering holographic interference. With QO model, we demonstrated that this difference is related to the ionization and rescattering times of the electron. Additionally, we showed that the Coulomb interaction does not matter for the oscillation of both the first-returning and second-returning holographic interferences. This allows us to measure the temporal characteristics of the electron in tunneling ionization by analyzing the relative phase dependence of the multiple-returning holographic interference.

Acknowledgements This work was supported by the National Natural Science Foundation of China (11874163, 11622431, 61475055,11604108, 11627809) and Program for HUST Academic Frontier Youth Team.

References

Agueny, H., Hansen, J.: High-order photoelectron holography in the midinfrared-wavelength regime. Phys. Rev. A **98**, 023414 (2018)
Arbó, D., Persson, E., Burgdörfer, J.: Time double-slit interferences in strong-field tunneling ionization. Phys. Rev. A **74**, 063407 (2006)
Arbó, D., et al.: Interference of electron wave packets in atomic ionization by subcycle sculpted laser pulses. Phys. Rev. A **89**, 043414 (2014)
Arbó, D., et al.: Ionization of argon by two-color laser pulses with coherent phase control. Phys. Rev. A **92**, 023402 (2015)
Becker, W., Grabon, F., Kopold, R., Milošević, D., Paulus, G., Walther, H.: Above-threshold ionization: from classical features to quantum effect. Adv. At. Mol. Opt. Phys. **48**, 35 (2002)
Bian, X., et al.: Subcycle interference dynamics of time-resolved photoelectron holography with midinfrared laser pulses. Phys. Rev. A **84**, 043420 (2011)
Blaga, C., Catoire, F., Colosimo, P., Paulus, G., Muller, H., Agostini, P., DiMauro, L.: Strong-field photoionization revisited. Nat. Phys. **5**, 335–338 (2009)
Corkum, P.: Plasma perspective on strong field multiphoton ionization. Phys. Rev. Lett. **71**, 1994 (1993)
Du, H., Wu, H., Wang, H., Yue, S., Hu, B.: Theoretical scheme for simultaneously observing forward-backward photoelectron holography. Opt. Lett. **41**, 697–700 (2016)
Faisal, F.: Strong-field physics: ionization surprise. Nat. Phys. **5**, 319–320 (2009)
Feit, M., Fleck, J., Steiger, A.: Solution of the schrödinger equation by a spectral method. J. Comput. Phys. **47**, 412 (1982)
Ferray, M., et al.: Multiple-harmonic conversion of 1064 nm radiation in rare gases. J. Phys. B At. Mol. Opt. Phys. **21**, L31 (1988)
Gaarde, M., Schafer, K.: Quantum path distributions for high-order harmonics in rare gas atoms. Phys. Rev. A **65**, 031406 (2002)
Gabor, D.: A new microscopic principle. Nature **161**, 777 (1948)
He, Y., He, L., Lan, P., Wang, B., Li, L., Zhu, X., Cao, W., Lu, P.: Molecular rotation movie filmed with high-harmonic generation. arXiv:1902.05662 [physics.optics] (2019)
He, L., Lan, P., Le, A., Wang, B., Wang, B., Zhu, X., Lu, P., Lin, C.: Real-time observation of molecular spinning with angular high-harmonic spectroscopy. Phys. Rev. Lett. **121**, 163201 (2018a)
He, M., Li, Y., Zhou, Y., Li, M., Cao, W., Lu, P.: Direct visualization of valence electron motion using strong-field photoelectron holography. Phys. Rev. Lett. **120**, 133204 (2018b)
Hickstein, D., et al.: Direct visualization of laser-driven electron multiple scattering and tunneling distance in strong-field ionization. Phys. Rev. Lett. **109**, 073004 (2012)

Huismans, Y., et al.: Time-resolved holography with photoelectrons. Science **331**, 61 (2011)
Huismans, Y., et al.: Scaling Laws for Photoelectron Holography in the midinfrared wavelength regime. Phys. Rev. Lett. **109**, 013002 (2012)
Kang, H., et al.: Structure effects in angle-resolved high-order above-threshold ionization of molecules. Phys. Rev. Lett. **104**, 203001 (2010)
Krause, J., Schafer, K., Kulander, K.: High-order harmonic generation from atoms and ions in the high intensity regime. Phys. Rev. Lett. **68**, 3535 (1992)
Krausz, F., Ivanov, M.: Attosecond physics. Rev. Mod. Phys. **81**, 163 (2009)
Lein, M.: Atomic physics: electrons get real. Nature **485**, 313 (2012)
Li, X., Liu, W., Song, Y., Zhang, C., Long, H., Wang, K., Wang, B., Lu, P.: Enhancement of the Second Harmonic Generation from WS Monolayers by Cooperating with Dielectric Microspheres. Advanced Optical Materials **7**, 1801270 (2018)
Li, M., Xie, H., Cao, W., Luo, S., Tan, J., Feng, Y., Du, B., Zhang, W., Li, Y., Zhang, Q., Lan, P., Zhou, Y., Lu P.: Photoelectron holographic interferometry to probe the longitudinal momentum offset at the tunnel exit. Phys. Rev. Lett. (accepted)
Li, L., Lan, P., Zhu, X., Huang, T., Zhang, Q., Lein, M., Lu, P.: Reciprocal-space-trajectory perspective on high harmonic generation in solids. arXiv:1809.08109 [physics.optics] (2019a)
Li, J., Zhang, Q., Li, L., Zhu, X., Huang, T., Lan, P., Lu, P.: Orientation dependence of high-order harmonic generation in nanowire. Phys. Rev. A **99**, 033421 (2019b)
Lindner, F., et al.: Attosecond double-slit experiment. Phys. Rev. Lett. **95**, 040401 (2005)
Liu, C., Hatsagortsyan, K.: Origin of unexpected low energy structure in photoelectron spectra induced by midinfrared strong laser fields. Phys. Rev. Lett. **105**, 113003 (2010)
Liu, K., Luo, S., Li, M., Li, Y., Feng, Y., Du, B., Zhou, Y., Lu, P., Barth, I.: Detecting and characterizing the nonadiabaticity of laser-induced quantum tunneling. Phys. Rev. Lett. **122**, 053202 (2019)
Ma, X., Zhou, Y., Li, N., Li, M., Lu, P.: Attosecond control of correlated electron dynamics in strong-field nonsequential double ionization by parallel two-color pulses. Opt. Laser Technol. **108**, 235–240 (2018)
Ma, X., Zhou, Y., Chen, Y., Li, M., Li, Y., Zhang, Q., Lu, P.: Timing the release of the correlated electrons in strong-field nonsequential double ionization by circularly polarized two-color laser fields. Opt. Express **27**(3), 1825–1837 (2019)
Marchenko, T., Huismans, Y., Schafer, K., Vrakking, M.: Criteria for the observation of strong-field photoelectron holography. Phys. Rev. A **84**, 053427 (2011)
Meckel, M., Staudte, A., Patchkovskii, S., Villeneuve, D., Corkum, P., DÖrner, R., Spanner, M.: Signatures of the continuum electron phase in molecular strong-field photoelectron holography. Nat. Phys. **10**, 594 (2014)
Paulus, G., Nicklich, W., Xu, H., Lambropoulos, P., Walther, H.: Plateau in above threshold ionization spectra. Phys. Rev. Lett. **72**, 2851 (1994)
Qin, Y., Li, M., Li, Y., He, M., Luo, S., Liu, Y., Zhou, Y., Lu, P.: Asymmetry of the photoelectron momentum distribution from molecular ionization in elliptically polarized laser pulses. Phys. Rev. A **99**, 013431 (2019)
Quan, W., et al.: Classical aspects in above-threshold ionization with a midinfrared strong laser field. Phys. Rev. Lett. **103**, 093001 (2009)
Salières, P., et al.: Feynman's path-integral approach for intense-laser-atom interactions. Science **292**, 902–905 (2001)
Shar, D., Soifer, H., Bruner, B., Dagan, M., Mairesse, Y., Patchkovskii, S., Ivanov, M., Smirnova, O., Dudovich, N.: Resolving the time when an electron exits a tunneling barrier. Nature **484**, 343 (2012)
Smirnova, O., et al.: High harmonic interferometry of multi-electron dynamics in molecules. Nature **460**, 972–977 (2009)
Tan, J., Zhou, Y., He, M., Chen, Y., Ke, Q., Liang, J., Zhu, X., Li, M., Lu, P.: Determination of the ionization time using attosecond photoelectron interferometry. Phys. Rev. Lett. **121**, 253203 (2018a)
Tan, J., Zhou, Y., Li, M., He, M., Liu, Y., Lu, P.: Accurate measurement of laser intensity using photoelectron interference in strong-field tunneling. Opt. Express **26**, 020063 (2018b)
Tan, J., Zhou, Y., He, M., Ke, Q., Liang, J., Li, Y., Li, M., Lu, P.: Time-resolving tunneling ionization via strong-fieldphotoelectron holography. Phys. Rev. A **99**, 033402 (2019)
Tong, A., Li, Q., Ma, X., Zhou, Y., Lu, P.: Internal collision induced strong-field nonsequential double ionization in molecules. Optics Express **27**, 6415 (2019)
Walker, B., Sheehy, B., DiMauro, L., Agostini, P., Schafer, K., Kulander, K.: Precision measurement of strong field double ionization of helium. Phys. Rev. Lett. **73**, 1227 (1994)
Wang, R., Zhang, Q., Li, D., Xu, S., Cao, P., Zhou, Y., Cao, W., Lu, P.: Identification of tunneling and multiphoton ionization in intermediate Keldysh parameterregime. Opt. Express **27**, 6471–6482 (2019)

Xie, X., et al.: Attosecond probe of vlence-electron wave packets by subcycle sculpted laser fields. Phys. Rev. Lett. **108**, 193004 (2012)
Xie, H., Li, M., Li, Y., Zhou, Y., Lu, P.: Intra-half-cycle interference of low-energy photoelectron in strong midinfrared laser fields. Opt. Express **24**, 027726 (2016)
Yan, T., Popruzhenko, S., Vrakking, M., Bauer, D.: Low-energy structures in strong field ionization revealed by quantum orbits. Phys. Rev. Lett. **105**, 253002 (2010)
Zhai, C., Zhang, Y., Zhang, Q.: Characterizing the ellipticity of an isolated attosecond pulse. Opt. Commun. **437**, 104–109 (2019)
Zhang, X., Zhu, X., Wang, D., Li, L., Liu, X., Liao, Q., Lan, P., Lu, P.: Ultrafast oscillating-magnetic-field generation based on electronic-current dynamics. Phys. Rev. A **99**, 013414 (2019)
Zhou, Y., Huang, C., Lu, P.: Coulomb-tail effect of electron–electron interaction on nonsequential double ionization. Phys. Rev. A **84**, 023405 (2011a)
Zhou, Y., Huang, C., Tong, A., Liao, Q., Lu, P.: Correlated electron dynamics in nonsequential double ionization by orthogonal two-color laser pulses. Opt. Express **19**, 2301–2308 (2011b)
Zhou, Y., Tolstikhin, O., Morishita, T.: Near-forward rescattering photoelectron holography in strong-field ionization: extraction of the phase of the scattering amplitude. Phys. Rev. Lett. **116**, 173001 (2016)

Affiliations

Yali Liu[1] · Jia Tan[1] · Mingrui He[1] · Hui Xie[1] · Yanan Qin[1] · Yong Zhao[1] · Min Li[1] · Yueming Zhou[1] · Peixiang Lu[1,2]

Yali Liu
liuyali@hust.edu.cn

Jia Tan
jiat@hust.edu.cn

Mingrui He
hmr_emma@hust.edu.cn

Hui Xie
xiehuihust@hust.edu.cn

Yanan Qin
ynqin@hust.edu.cn

Yong Zhao
zy2018@hust.edu.cn

Min Li
mli@hust.edu.cn

Peixiang Lu
lupeixiang@hust.edu.cn

[1] School of Physics, Huazhong University of Science and Technology, Wuhan 430074, People's Republic of China

[2] Laboratory of Optical Information Technology, Wuhan Institute of Technology, Wuhan 430205, People's Republic of China